Electrochimica Acta 362 (2020) 137094

Contents lists available at ScienceDirect

Electrochimica Acta

journal homepage: www.elsevier.com/locate/electacta

Research Article

Simultaneous voltammetric detection of six biomolecules using a nanocomposite of titanium dioxide nanorods with multi-walled carbon nanotubes

Bhargav R. Patel, Saim Imran, Wanying Ye, Hanyi Weng, Meissam Noroozifar, Kagan Kerman*

Department of Physical and Environmental Sciences, University of Toronto Scarborough, 1265 Military Trail, Toronto, ON, M1C 1A4, Canada

ARTICLE INFO

Article history:
Received 25 June 2020
Revised 13 August 2020
Accepted 9 September 2020
Available online 14 September 2020

Keywords:
Electrochemical sensor
Titanium dioxide nanorods
Multi-walled carbon nanotubes
Nanocomposite
Simultaneous determination
Differential pulse voltammetry
Cyclic voltammetry

ABSTRACT

In this proof-of-concept study, a novel nanocomposite of titanium dioxide nanorods with multi-walled carbon nanotubes (TiO_2NRs-MWCNTs) was synthesized using a solvo-thermal method and characterized by transmission electron microscopy (TEM) and Fourier-transform infrared spectroscopy (FTIR). The nanocomposite of TiO_2NRs-MWCNTs was utilized to modify the surface of a glassy carbon electrode (GCE) using 1.5% (v/v) Nafion^{TM} solution for a proof-of-concept study to detect uric acid (UA), xanthine (XA), theophylline (TP) and theobromine (TB) in the presence of ascorbic acid (AA) and dopamine (DA). Simultaneous detection of these six biomolecules was performed using differential pulse voltammetry (DPV) in a wide potential window from -0.3 V to -1.6 V (*vs.* Ag/AgCl) at pH 4.0. The TiO_2NRs-MWCNTs/GCE showed strong, stable and six simultaneous well-separated anodic peaks at 0.13, 0.35, 0.50, 0.85, 1.10 and 1.28 V for AA, DA, UA, XA, TP and TB, respectively. The calibration curves showed linearity to 191.0, 147.0, 537.0, 586.0, 893.0, 1653.0 µM with detection limits of 0.51, 0.06, 0.05, 0.09, 0.56 and 0.75 µM for AA, DA, UA, XA, TP and TB, respectively. The electrochemical performance of the TiO_2NRs-MWCNTs/GCE displayed good reproducibility for simultaneous determination of six analytes. Finally, our preliminary results suggested that the TiO_2NRs-MWCNTs/GCE can provide a promising platform for rapid quantitative detection of AA, DA, UA, XA, TP and TB in quality control studies of real samples such as pharmaceuticals and food products.

1. Introduction

Simultaneous detection using electrochemical sensors are emerging as a powerful technique for quality control assays, mass production and on-field rapid tests for environmental studies due to their high accuracy, selectivity, reproducibility, low cost and simple operation [1]. Hence, they have been widely employed in quantitative measurement of the biomolecules and drugs in industrial settings [2]. The sensitive and rapid quantitative detection of these biomolecules also benefits pathological research, clinical diagnosis and pharmaceutical quality control [3–5]. Ascorbic acid (AA) and dopamine (DA) are related to cognitive wellness, while uric acid (UA), xanthine (XA), theophylline (TP), and theobromine (TB) are products in the purine metabolism pathway; hence all the mentioned compounds represent important roles in the body. Lack of AA increases the risk of scurvy [6], while DA is a catecholamine neurotransmitter found in the central nervous system. It is involved in the regulation of voluntary movement and reward value [7,8]. Past research has shown that inadequate dopamine levels can cause Parkinson's diseases and attention-deficit hyperactivity disorder (ADHD) [9–11]. Purines are a class of heterocyclic aromatic organic compounds including UA, XA, TP, and TB that contain a pyrimidine ring fused with the imidazole ring structure [12]. TB and TP are neuro-stimulants, which can be formed from xanthine (XA) as the precursor (Scheme 1) [13,14]. High UA concentration in urine is reported to be a sign of hyperuricemia which is known to progress into gout [15]. Scheme 1 illustrates how the purine compounds such as TB, TP, and XA can be produced from degradation of the precursor molecule, xanthosine, a xanthine-based nucleoside, through different metabolic pathways. It also shows that UA is the final oxidized product of the hypothesized purine catabolism pathway [16]. Depending on which enzyme is used, either nucleosidase or 7-methylxanthosine synthase with S-adenosyl-L-methionine (SAM), the formation of XA or 7-methylxanthine can occur, respectively (Scheme 1). Furthermore,

* Corresponding author:
E-mail address: kagan.kerman@utoronto.ca (K. Kerman).

https://doi.org/10.1016/j.electacta.2020.137094
0013-4686/

methylation with SAM reduction to S-adenosyl-L-homocysteine (SAH) can produce TP or TB, respectively [17]. TB and TP can be converted back to XA upon the action of N-demethylase in the liver, while XA can then be oxidized to UA by xanthine oxidase [18,19]. Since, these biomolecules usually co-exist in real-life samples, such as urine, simultaneous detection can be of paramount significance. Therefore, it is physiologically relevant and essential to perform the simultaneous determinations of these compounds with high sensitivity and selectivity.

However, the challenge of simultaneous detection is the fusion of electrooxidation peaks of different biomolecules due to the oxidative potentials of them being close to each other, which results in a single indistinguishable peak. Subsequently, nanocomposite modified electrodes have been used to produce better separation and resolution of oxidation peaks during simultaneous detection of up to six different redox-active compounds [20–25]. AA, DA, UA and XA have been simultaneously detected by multiple electrodes. Ganesh et al. [20] successfully developed epigallocatechin gallate-modified graphite paste electrode for simultaneous detection of AA, DA and UA. Shastan et al. [21] detected four compounds AA, DA, UA and Trp (Trptophan) simultaneously by buckyball-modified carbon-ceramic microelectrodes (CCMEs). Jesny and Kumar [22] used modified GCE with an electropolymerized layer of para-amino benzene sulfonic acid to achieve simultaneous detection of XA, TP, and caffeine (CA). Furthermore, Hossieny and Yassien [23] also fabricated a nano-boron doped ceria modified glassy carbon paste electrode to detect AA, DA, UA and XA, simultaneously. However, only a very few studies have been reported about the simultaneous electrochemical detection of more than four redox-active biomolecules. Recently, Wang et al., [24] developed chemical vapor deposition (CVD) graphene-based electrochemical sensor for simultaneous detection of five biomolecules (AA, DA, UA, Trp, and NO_2^-). In addition, Li et al. [25] used ferricyanide-doped chitosan and multi-walled carbon nanotubes (MWCNTs) nanocomposite-modified graphite paste electrode for simultaneous detection of AA, DA, UA, Trp, XA and CA. To the best of our knowledge, the work of Li et al. [25] has been the only reported study so far to achieve the simultaneous detection of six redox-active biomolecules with well-separated and well-defined oxidation peaks. In this study, TB and TP were detected using voltammetry, whereas these biomolecules would generally require bench-top HPLC and UV array systems for quantitative analysis [26,27]. To the best of our knowledge, despite having similar structures and co-existing in real samples, simultaneous electrochemical detection of both TB and TP has been reported by Spătaru et al. [28]. Recently, Švorc et al. [29], used miniaturized boron-doped diamond electrodes for voltammetric detection of TB in chocolate products. Moreover, TP has been electrochemically detected in the presence of XA and CA by Jesny and Girish [22]. Therefore, this work would be only the second one to achieve simultaneous detection of six biomolecules and the first one which can simultaneously detect AA, DA, UA, XA, TP and TB.

The glassy carbon electrode (GCE) surface can be modified by casting of novel nanocomposite materials to improve the overall selectivity and sensitivity of the electrode to target analytes [30]. Furthermore, GCE presents great electrocatalysis value due to low reactivity, high temperature tolerance, strong hardness, impermeability and high electrical conductivity [31]. A nanocomposite of titanium dioxide nanorods (TiO_2NRs) and multi-walled carbon nanotubes (MWCNTs) was used to modify the surface of a GCE (TiO_2NRs-MWCNTs/GCE). TiO_2-based nanomaterials present great potential for use in electrochemical detection of biomolecules due to its stability, non-toxicity, and biocompatibility [32]. Also, their mesoporous internal structure gives promising electron-accepting property that enables TiO_2 to collect electrons produced by oxidation of biomolecules during electrochemical measurements [32]. TiO_2 nanomaterials have been routinely used in electrode surface modifications, as they present large surface area and enhanced electrocatalytic properties, while requiring only mild temperature conditions for synthesis [33]. Among the previously synthesized TiO_2-based nanomaterials, TiO_2NRs have been characterized to show properties of one-dimensional nanostructures with large surface-to-volume area as excellent electron transfer mediators [34,35]. MWCNTs are also widely used in the synthesis of nanocomposites due their high chemical stability, electrical conductivity and large surface area [36]. Previous studies [25,37] have shown that the electrode modification with MWCNTs can largely increase electron and proton transferring rate, giving rise to better peak separation, and improved electrode sensitivity than other modified electrodes. Nafion (NF) is a polymer extensively used in sensors due to its electrocatalytic properties [38], as it provides a connection for proton transfer from its sulfonic groups to the perfluorinated hydrophobic backbone [39]. Therefore, NF was used for binding the TiO_2NRs-MWCNTs nanocomposite onto the activated surface of GCE. Furthermore, researchers have found that GCE modified with both nanomaterials and NF has a better electrochemical performance than GCE modified with solely nanomaterials [40]. In this study, the TiO_2NRs-MWCNTs nanocomposite was synthesized by a solvo-thermal method, which employed an ultrasonic bath to pre-disperse the solid-liquid matrix instead of stirring the matrix during overnight autoclaving. A solution of TiO_2NRs and MWCNTs underwent a solvo-thermal treatment forming the TiO_2NRs-MWCNTs as a nanocomposite. Finally, a mixture of TiO_2NRs-MWCNTs with NF, as the binding agent, was used for preparation of nanocomposite modified GCEs. The TiO_2NRs-MWCNTs/GCE was used for the simultaneous electrochemical measurements using DPV. To the best of our knowledge, there is no study that has reported a nanocomposite-based electrochemical sensor capable of simultaneously detecting TB and TP in the presence of AA, DA, XA and UA. In addition, recovery tests of the six analytes were completed using real samples of cocoa products and physiologically relevant matrices such as urine samples. The TiO_2NRs-MWCNTs/GCE presented enhanced stability, reproducibility, selectivity and sensitivity during detection of all six analytes.

2. Experimental

2.1. Materials

L-Ascorbic acid (AA, ≥ 99% crystalline), dopamine hydrochloride (DA, ≥ 98%), uric acid (UA, ≥ 99% crystalline), xanthine (XA, ≥ 99%), anhydrous theophylline (TP, ≥ 99% powder), theobromine (TB, ≥ 98%), multi-walled carbon nanotubes (MWCNTs, OD of 20–30 nm with a wall thickness of 1–2 nm and length ranging from 0.5 to 2 μm with purity of ≥ 95%), and TiO_2 nanoparticles (21 nm with purity ≥ 99.5%) and Nafion-117 were purchased from Sigma-Aldrich (Oakville, ON).

2.2. Instruments

All electrochemical measurements were performed using μAutolab PGSTAT 128 N (Metrohm-EcoChemie, Utrecht, The Netherlands) potentiostat/galvanostat, that was controlled by NOVA™ 2.1 (Metrohm-EcoChemie, Utrecht, The Netherlands) software connected to a three-electrode cell. The TiO_2NRs-MWCNTs/GCE was utilized as the working electrode, while platinum wire acted as the auxiliary electrode, and a saturated Ag/AgCl electrode was the reference electrode. All measurements were conducted at room temperature. The DPV potential window was optimized and set from −0.3 to 1.6 V at a step potential of 5 mV and modulation amplitude of 0.025 V with a modulation time of 0.05 s as well as an interval time of 0.5 s. The morphology of the nanocomposites

was characterized through TEM using Hitachi H-7500 transmission electron microscope (Hitachi, Japan). Bruker alpha-P FT-IR spectrometer (Billerica, MA) having deuterated lanthanum α alanine doped triglycine sulfate (DLaTGS) detector was used to obtain the FT-IR spectra. Powdered MWCNTs, TiO_2NPs, TiO_2NRs, and TiO_2NRs-MWCNTs nanocomposite were placed on the crystal to generate the FT-IR spectrum. FT-IR spectra were obtained at a resolution of 2 cm^{-1} at a scan rate of 16, between 4000 cm^{-1} to 360 cm^{-1}. FT-IR spectra were baseline corrected and smoothened once with an average of 17 data points. Opus 6.5® software was used to perform all the FT-IR spectral data analysis.

2.3. Preparation of reagents

The stock solutions (5.0 mL) of 0.1 M AA and DA were prepared directly using sterile 18.2 μΩ ultra-pure water obtained from Cascada LS water purification system (Pall Co., Mississauga, ON). In addition, the stock solutions (5.0 mL) of 0.01 M UA, XA, TP, and TB were also prepared using ultra-pure water and the pH was adjusted with 15 μL of 10 M NaOH. Furthermore, 0.2 M phosphate electrolyte solution was prepared from H_3PO_4 (14.8 M), and the desired pH range (pH 2.0–5.0) was adjusted using 10 M NaOH, while the buffer solutions with higher pH range were prepared by equimolar mixing of K_2HPO_4 with KH_2PO_4 solutions, then the desired pH range (pH 6.0–8.0) was adjusted using 4.0 M HCl solution.

2.4. Synthesis of TiO_2NRs and TiO_2NRs-MWCNTs

TiO_2NRs-MWCNTs were prepared by mixing 200 mg TiO_2 nanoparticles and 50 mg MWCNTs with 10.0 mL of concentrated NaOH solution in a scintillation vial. The mixture was placed in an ultrasonic bath for 30 min at 60 °C and was then transferred to a Teflon-lined stainless-steel autoclave container and kept at 130 °C for 24 h. The resulting nanocomposite was washed with 1.0 L ultra-pure water and neutralized to pH 7.0 with 0.1 M HCl, followed by a thorough washing with 0.5 L ultra-pure water. Finally, the nanocomposite was dried at 80 °C for 24 h. TiO_2NRs were similarly prepared with the exception that initially step did not include the addition of 50 mg MWCNTs.

2.5. Preparation of the modified GCEs with TiO_2NRs-MWCNTs

The surface of GCE was cleaned by polishing with micro-polish Gamma Alumina powder for 15 mins and activated in 0.5 M H_2SO_4 using cyclic voltammetry (CV). A desired amount (5 mg) of TiO_2NRs-MWCNTs nanocomposite was mixed with an aliquot (100 μL) of 1.5% (v/v) Nafion™ solution in a scintillation vial, which was then dispersed for 30 mins in an ultrasonic bath at 60 °C. An aliquot (2 μL) of the resulting solution was drop-cast on the activated GCE surface and left to dry under IR radiation for 30 min. For the purpose of electrochemical performance comparison studies to check the effectiveness of the modified electrodes, TiO_2NRs/GCE and MWCNTs/GCE were also prepared with the same methods described above and compared with each other as well as with the bare GCE surfaces.

2.5. Preparation of real samples

Urine samples were collected from a healthy individual and used following the ethical guidelines. All procedures using real samples were approved for the project no. 950–231116 by the Research Ethics Committee of the University of Toronto and were in accordance with the guidelines and codes established by the Interagency Advisory Panel on Research Ethics (PRE). An aliquot (1 mL) of urine solution was added to a scintillation vial and diluted five-fold using 0.2 M PBS (pH 4.0). The diluted urine samples were then mixed with known concentrations of AA, DA, XA, TP and TB using the standard addition method to prepare the spiked urine sample solutions. A commercially available chocolate powder was used to prepare a stock concentration of 0.133 g/mL in distilled water. The solution was heated while stirring continuously on a hotplate for 24 h. After cooling down, the solution was diluted five-fold using 0.2 M PBS (pH 4.0) followed by the standard addition of six target biomolecules as described above.

3. Results and discussion

3.1. Characterization of the nanocomposite

Particle morphology for TiO_2NPs, TiO_2NRs and TiO_2 NRs-MWCNTs are shown as TEM images in Fig. 1. The rod-like structures of TiO_2NRs (as shown in Fig. 1b) indicated the successful formation of TiO_2NRs from the initial sphere-like structures of TiO_2NPs observed in Fig. 1a. Additionally, the TEM images of TiO_2NRs-MWCNTs in Fig. 1c and 1d showed the combination of the MWCNTs with the TiO_2NRs.

The FTIR spectrum of MWCNTs showed peaks at 1544, 1951, 2118, 2328 and 2665 cm^{-1} indicates $C = C$ stretching, O–H deformation vibrations, $C = O$ stretching, C–OH stretching and C–H stretching, respectively [41,42]. The peaks at 437 and 734 cm^{-1} in FTIR spectrum of TiO_2NPs are the contributions of the anatase phase of TiO_2NPs as reported by Karakitsou & Verykios [43,44]. In the FTIR spectrum of TiO_2NRs, the intense broad peak at 3251 was characteristic of the O–H stretching vibrations, the band around 1633 cm^{-1} represented the deformative vibration of Ti-OH stretching mode, and the band around 930 cm^{-1} indicated the stretching vibration of short Ti-O bonds incorporating non-bridging oxygen. The weak peak at 694 cm^{-1} was again a contribution of the anatase phase of TiO_2, while the sharp and intense peak at 445 cm^{-1} represented Ti-O bending mode [35,45]. Finally, for the TiO_2NRs-MWCNTs, the characteristic sharp peak of Ti-O bending mode was split into two peaks at 444 and 415 cm^{-1}, in addition, peaks at 939, 2117, and the broad peak at 3211 cm^{-1} were indicative of the stretching vibration of short Ti-O bonds incorporating non-bridging oxygen, $C = O$ stretching, and O–H stretching vibrations, respectively.

3.2. Comparison of the electrochemical behavior of GCE, MWCNTs/GCE, TiO_2NRs/GCE and TiO_2NRs-MWCNTs/GCE

The electrochemical responses of the modified electrodes and the bare GCE were studied in a mixture of AA, DA, UA, XA, TP, and TB. As shown in Fig. 2, the bare GCE was able to detect only UA, TP and TB with the oxidation peak potentials at 0.50, 1.13 and 1.31 V, however, the oxidation peaks were low and broad, which suggested slow electron transfer kinetics. In addition, both MWCNTs/GCE and TiO_2NRs/GCE showed very broad and low oxidation peaks for all six biomolecules at specified concentrations. However, under the same experimental conditions, DPV of the TiO_2NRs-MWCNTs/GCE provided the detection of all six analytes and showed substantial increase in the anodic peak current at 0.13, 0.35, 0.50, 0.85, 1.10 and 1.28 V, for AA, DA, UA, XA, TP and TB, respectively. Moreover, with TiO_2NRs-MWCNTs/GCE displayed well-defined oxidation peaks, demonstrating the remarkable sensitivity of this novel sensor.

3.3. Redox-active surface area of TiO_2NRs-MWCNTs/GCE

The redox-active surface area (A) was calculated using the TiO_2NRs-MWCNTs/GCE and bare GCE. All the measurements were performed using CV between potentials of −0.2 to 0.8 V at varying scan rates. The anodic peak current (I_{pa}) from the respective

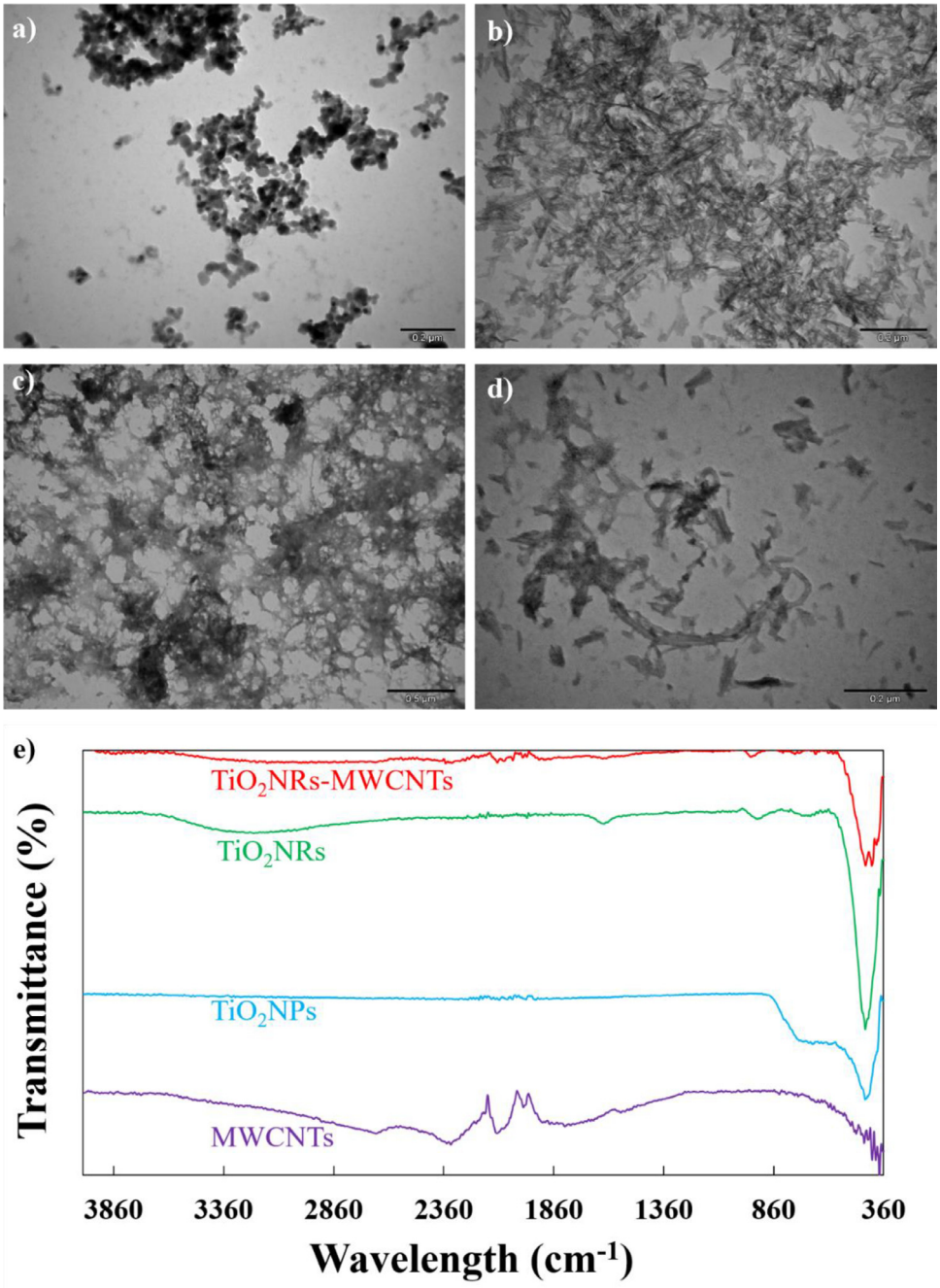

Fig. 1. TEM images of (a) TiO_2NPs, (b) TiO_2NRs, (c) TiO_2NRs-MWCNTs (low magnification) and (d) c with higher magnification. Scale bars indicate 0.2 μm for (a), (b), (d), and 0.5 μm for (c). e) FTIR of MWCNTs, TiO_2NPs, TiO_2NRs, and TiO_2NRs-MWCNTs nanocomposite.

CVs were obtained in the presence of 1 mM of $[Fe(CN)_6]^{3-/4-}$ in 0.1 M KCl as the supporting electrolyte (Fig. S3) and were plotted against the square root of scan rate (v). The linear relationship between the increasing I_{pa} *vs* $v^{1/2}$ indicated the presence of a diffusion-controlled process. Furthermore, in a reversible process, the Randles–Sevcik equation can be used as follows [46]:

$$I_{pa} = \left(2.69\ x\ 10^5\right) n^{3/2} D^{1/2} C A v^{1/2} \quad (1)$$

where I_{pa} refers to the anodic peak current, n is the electron transfer number, A is the active surface area of the electrode, D is the diffusion coefficient, C is the concentration of $[Fe(CN)_6]^{3-/4-}$ and v is the scan rate. For $[Fe(CN)_6]^{3-/4-}$, $n = 1$ and $D = 7.6 \times 10^{-6}$ cm s^{-1}; the active surface areas of the electrodes were calculated using the slope of the I_{pa}–$v^{1/2}$ plot. For the bare GCE and TiO_2NRs-MWCNTs/GCE, the active surface areas were calculated to be 0.05 and 0.31 cm^2, respectively. In order to better assess the effect of nanocomposite modification on the redox-active surface area, an estimation of the roughness factor (f_r) was performed. The roughness factors of the bare GCE and TiO_2NRs-MWCNTs/GCE were determined on the basis of the current of $[Fe(CN)_6]^{3-/4-}$ redox as a reversible process (Fig. S3). The measurements were carried out by means of CV in the same solution. Based on Randles–Sevcik equation for the reversible processes, all parameters are similar except active surface areas, A_1 and A_2, for bare GCE and TiO_2NRs-MWCNTs/GCE, respectively. Also, under the same conditions, I_{p1} and I_{p2} were peak currents of the unmodified and modified electrodes, respectively. The $\frac{Ip2}{Ip1}$ is equal to $\frac{A2}{A1}$ and describes the redox-active surfaces by rough-

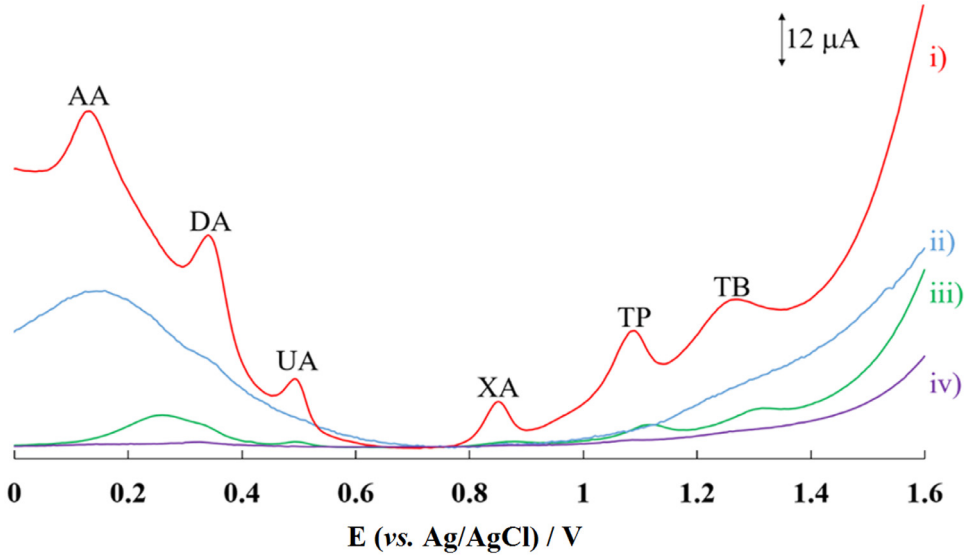

Fig. 2. DPV at the surface of i) TiO_2NRs-MWCNTs/GCE (red curve), ii) TiO_2NRs/GCE, iii) MWCNTs/GCE and iv) bare GCE, tested in a mixture of AA (97.0 μM), DA (2.5 μM), UA (2.5 μM), XA (5.0 μM), TP (20.0 μM), and TB (35.0 μM) in 0.2 M PBS at pH 4.0. (For interpretation of the references to colour in this figure legend, the reader is referred to the web version of this article.)

ness factor ($f_r = \frac{A2}{A1} = \frac{Ip2}{Ip1}$) [47,48]. As a result, an average f_r was estimated at 6.2 ± 0.05, which indicated that the modification of GCE with the TiO_2NRs-MWCNTs nanocomposite significantly increased the redox-active surface area. An EIS study was also performed to determine the capacitance of nanocomposite-modified GCEs. Fig. S3d represents the Nyquist plots of the bare GCE and TiO_2NRs-MWCNTs/GCE. The Nyquist plots showed that the charge-transfer resistance (R_{ct}) values of GCE and TiO_2NRs-MWCNTs/GCE were 993.7 ± 2.1 and 352.5 ± 1.9 Ω, respectively. Upon fitting the Nyquist plots with the modified Randles equivalent circuit shown in the inset of Fig. S3d, the R_{ct} of TiO_2NRs-MWCNTs/GCE was determined to be lower than that of the bare GCE. An estimated exchange current (I_0) can be used for comparison of the catalytic activity. The exchange current was calculated using $I_0 = \frac{R \times T}{n \times F \times Rct}$ where *R, T, n* and *F* are gas constant, absolute temperature, number of transferred electrons ($n = 1$) and Faraday constant, respectively. Based on this equation, the I_0 values for the bare GCE and TiO_2NRs-MWCNTs/GCE were calculated as 2.6 ± 0.10 and 7.3 ± 0.14 mA, respectively.

3.4. Simultaneous and individual determinations of six biomolecules

The electrochemical detection of six biomolecules was achieved by conducting simultaneous and individual DPV measurements using the TiO_2NRs-MWCNTs/GCE. The electrooxidation peak potentials of AA, DA, UA, XA, TP and TB were found to be at 0.13, 0.35, 0.50, 0.85, 1.10 and 1.28 V, respectively. The separation between each anodic peak were significant enough to provide the simultaneous detection of six biomolecules in a mixed solution (Fig. 3-red curve). Importantly, the oxidation peak potentials of AA (Fig. 3-brown line), DA (Fig. 3-black line), UA (Fig. 3-green line), XA (Fig. 3-pink line), TP (Fig. 3-purple line) and TB (Fig. 3-blue line) observed in individual test were detected at similar anodic peaks under same conditions.

3.5. pH effect and the hypothesized electrooxidation mechanisms of six biomolecules

We hypothesized that the acidity of electrolyte affected the anodic peak potentials of biomolecules significantly, since the protons took part in the surface reactions. The pH effect was studied in the pH range from 2.0 to 8.0 using the TiO_2−MWCNTs/GCE. The results in Fig. 4a indicated that as pH increased from pH 2.0 to 8.0, the peak potentials of AA, DA, UA, XA, TP, and TB moved towards less positive values. When the anodic peak potential *vs.* pH was plotted in Fig. 4b, the slopes of AA, DA, UA, XA, and TP were 0.0482, 0.0521, 0.0591, 0.0571, 0.0493 V/pH, respectively. These values were close to Nernstian slope of 0.059 V/pH and this indicated an equal proton-electron (*i.e.* two-proton and two-electron) transfer mechanism for the oxidation of these compounds, which was in good agreement with the literature [25,27,28,49,50]. The anodic peak potential shift with increasing pH for AA, DA, UA, XA, TP, and TB displayed a linear trend as shown in the Eqs. (2)–7:

$$E_p(AA) = -(0.0482 \pm 0.012)x + (0.3392 \pm 0.017)\ (R^2 = 0.9910) \quad (2)$$

$$E_p(DA) = -(0.0521 \pm 0.009)x + (0.5327 \pm 0.010)\ (R^2 = 0.9962) \quad (3)$$

$$E_p(UA) = -(0.0591 \pm 0.013)x + (0.7010 \pm 0.013)\ (R^2 = 0.9962) \quad (4)$$

$$E_p(XA) = -(0.0571 \pm 0.023)x + (1.0576 \pm 0.021)\ (R^2 = 0.9907) \quad (5)$$

$$E_p(TP) = -(0.0493 \pm 0.014)x + (1.3088 \pm 0.032)(R^2 = 0.9962) \quad (6)$$

$$E_p(TB) = -(0.0216 \pm 0.011)x + (1.4374 \pm 0.035)\ (R^2 = 0.9962) \quad (7)$$

As shown in Fig. 4a, pH 4.0 displayed higher anodic peak current signals and the best peak separations, therefore, it was selected as the optimal pH for further studies.

The hypothesized mechanisms are shown in Eqs. (8)–13 for AA, DA, UA, XA, TP, and TB respectively. However, TB seemed to be

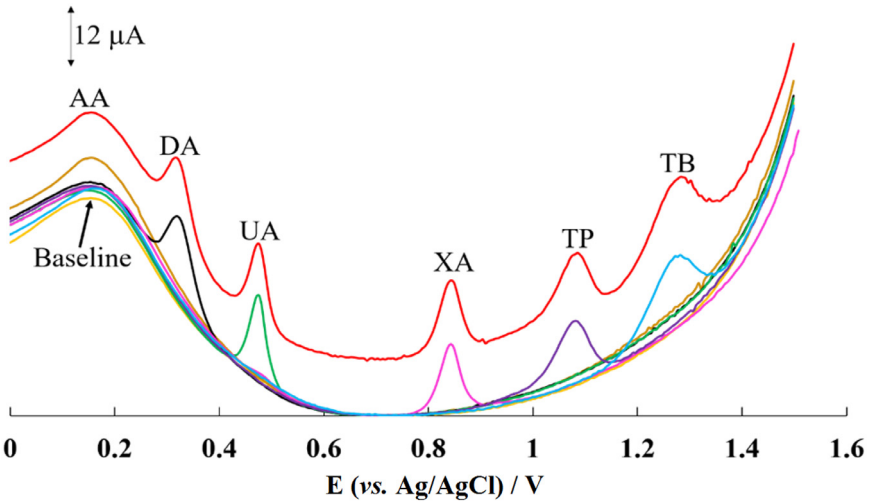

Fig. 3. DPV of the background (blank 0.2 M PBS, yellow line), individual solutions of AA (97.0 μM, brown line), DA (2.5 μM, black line), UA (5.0 μM, green line), XA (7.5 μM, pink line), TP (20.0 μM, purple line), TB (35.0 μM, blue line), and for mixture of all of them (red line) in 0.2 M PBS (pH 4.0). (For interpretation of the references to colour in this figure legend, the reader is referred to the web version of this article.)

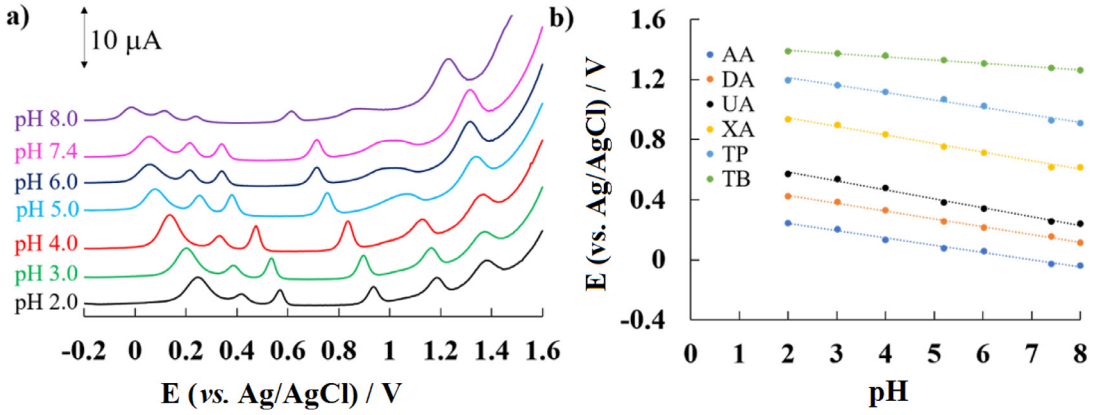

Fig. 4. (a) DPV of TiO_2NRs-MWCNTs/GCE recorded in the presence of AA (125.0 µM), DA (12.0 µM), UA (17.0 µM), XA (17.0 μM), TP (58.0 µM), and TB (160.0 µM) simultaneously in 0.2 M PBS at pH 2.0, 3.0, 4.0, 5.0 6.0, 7.0 and 8.0. (b) Linear regression plots of anodic peak potential *vs.* pH for six biomolecules.

an exception as it displayed a slope of 0.0216 V/pH, which suggested that the electrooxidation mechanism included a ratio of 1 proton to 3 electrons during the redox process. This initially refutes the expected result for a mildly acidic buffer (0.2 M PBS, pH 4), however, compared to previous literature, there is strong evidence showing that TB did not follow the direct relationship between pH and proton involvement as observed with AA, DA, UA, XA, or TP [22,25,28,29,51]. Moreover, it was reported to follow a similar mechanism as caffeine, where the oxidation would take place over two steps with the first being the rate determining step [28,52,53].

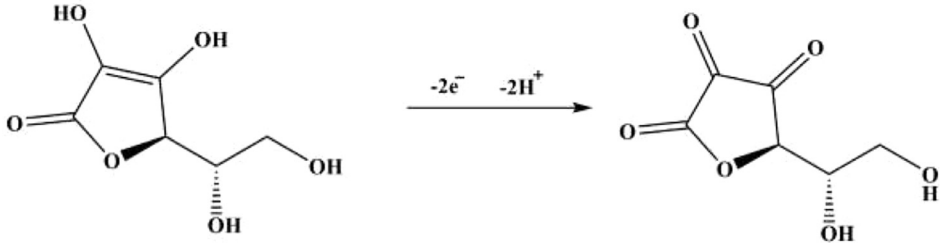

(8)

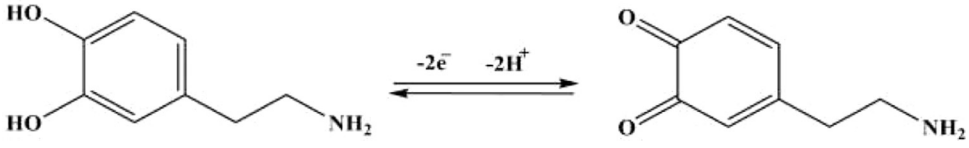

(9)

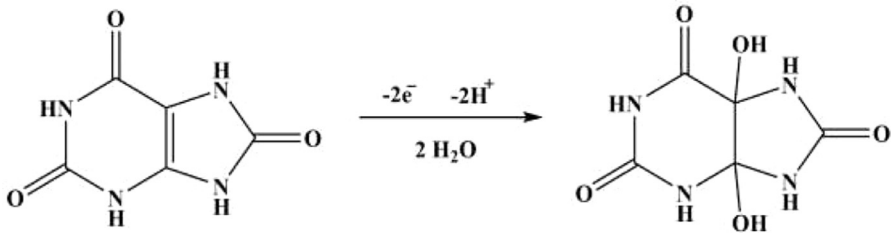

(10)

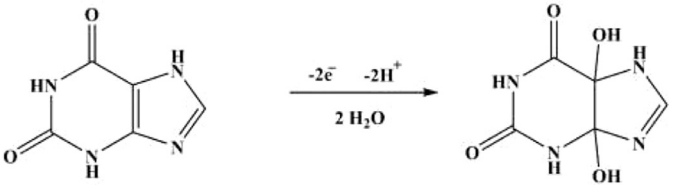

(11)

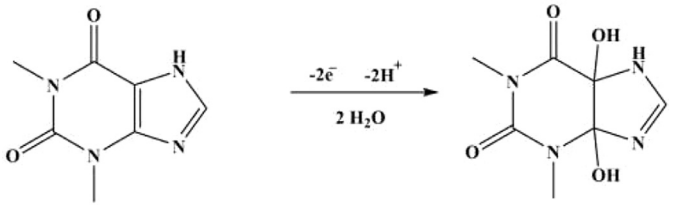

(12)

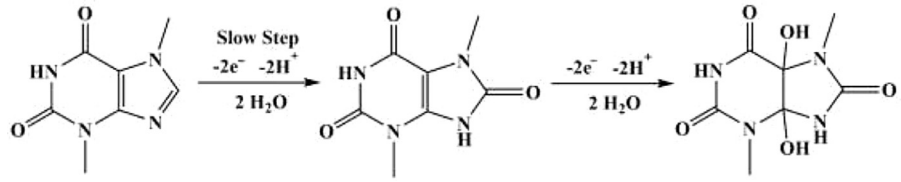

(13)

The limit of determination (LOD) of the six biomolecules was calculated using the equation: LOD = 3 × S_{blank}/m, where S_{blank} represents the standard deviation of background signals (n = 10) of the TiO_2NRs-MWCNTs/GCE, and m is the slope of the calibration curve from the first segment. The theoretical LOD for AA, DA, UA, XA, TP and TB were calculated to be 0.51, 0.06, 0.05, 0.09, 0.56 and 0.75 μM, respectively. The unique redox properties and the high electron transfer kinetics due to the increased surface area obtained from the TiO_2NRs-MWCNTs nanocomposite enabled the enhanced analytical performance of the sensor According to the prior literature, the pK_a values of DA, UA, AA, XA, TP and TB are 8.86, 5.8, 4.19, 7.4, 8.8, 10.0, respectively [55-58]. In an environment where pH is lower than pK_a values of the biomolecules, the biomolecules will be in their protonated form, therefore, at the pH 4.0, DA, UA, AA, XA, TP, and TB will mostly exist as cations [55,59]. This facilitates the electrostatic interactions of the cationic forms of DA, UA and AA with the negatively charged sulfonic acid (SO_3^-) functional groups of Nafion and COO^- groups of MWCNTs at pH 4.0, which is consistent with previous literature [60,61]. In addition, according to Cheng et al. [61], specifically for DA, the presence of phenyl groups enables the π-π interactions with MWCNTs, which would assist in the peak separation between AA, DA, and UA. Finally, the presence of TiO_2NRs-MWCNTs nanocomposite provides excellent electrocatalytic activity which also facilitates the detection of DA, UA and XA. However, DA forms an electro-polymerised film due to electrooxidation at the electrode surface that leads to electrode fouling or poisoning [62,63]. This is commonly observed due the requirement of high overpotential [61,64]. Moreover, indistinguishable and overlapping oxidation peaks for target analytes can be observed in the absence of modifications at the electrode surfaces [65,66]. Past studies have indicated that one of the ways to overcome electrode fouling from a biological substrate is by modifying the surfaces using chemical compounds (*i.e.* polyethylene glycol, PEG) and nanocomposites [62]. Kumar et al. [64] have demonstrated that the presence of nano-TiO_2 in the nanocomposite played an important role in improving the antifouling properties. Therefore, modifying the surfaces using Nafion, MWCNTs and TiO_2NRs significantly improved the selectivity and electrocatalytic properties of the sensors [64,67–70]. A comparison of our nanocomposite-modified sensor with the ones in literature is shown in Table 1. Based on the comparison shown in the table, the TiO_2NRs-MWCNTs/GCE showed a relatively larger linear dynamic range especially for AA, XA, TP and TB, while it also had comparable or better LOD for all

3.6. Calibration

DPV measurements were performed to explore the relationship between the anodic peak currents and concentrations of AA, DA, UA, XA, TP and TB. The measurements continued until the saturation was reached, and the peaks began to fuse with each other or did not increase as the concentrations increased. The results of the concentration-dependence study for simultaneous detection are shown in the Fig. 5, as six well-distinguished anodic peaks.

For each biomolecule, the anodic peak currents were subtracted by the background current (measured in blank PBS) of GCE-TiO_2NRs-MWCNTs to calculate ΔI, and ΔI (μA) was plotted against the concentration (μM) of the biomolecules. The plot of anodic peak current *vs* the increasing concentrations of AA, DA, UA, XA, TP and TB are shown in Fig. 6. All six calibration curves showed two segments of linear relationship, with a slope for low concentrations and a slope for higher concentrations. This was attributed to the difference in the availability of redox-active area on the electrode surface. We hypothesized that a large redox-active area was accessible on the electrode surface at lower concentrations of the biomolecules. However, at higher concentrations of the biomolecules, the accessible redox-active areas were rapidly saturated, and this resulted in the reduced sensitivity of the slope in the second linear segments for all six biomolecules [21,25,54].

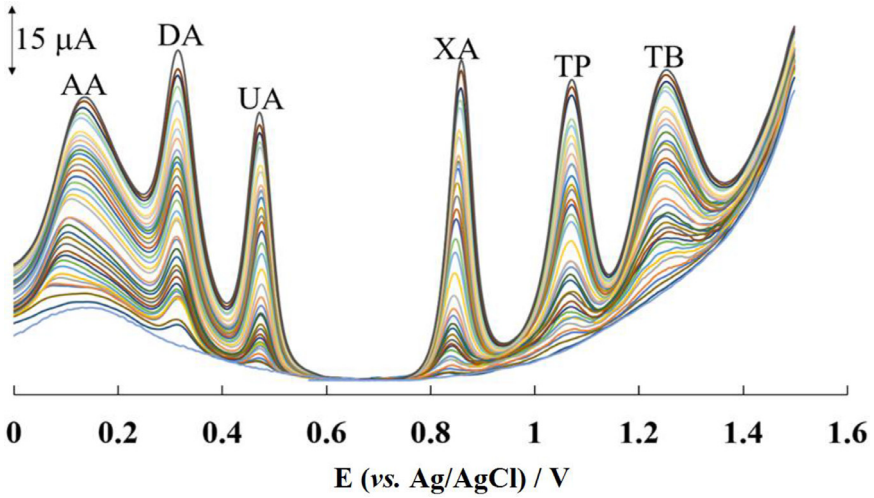

Fig. 5. DPV measurements for the simultaneous detection of AA, DA, UA, XA, TP, and TB at varying concentrations using the TiO_2NRs-MWCNTs/GCE in 0.2 M PBS (pH 4.0).

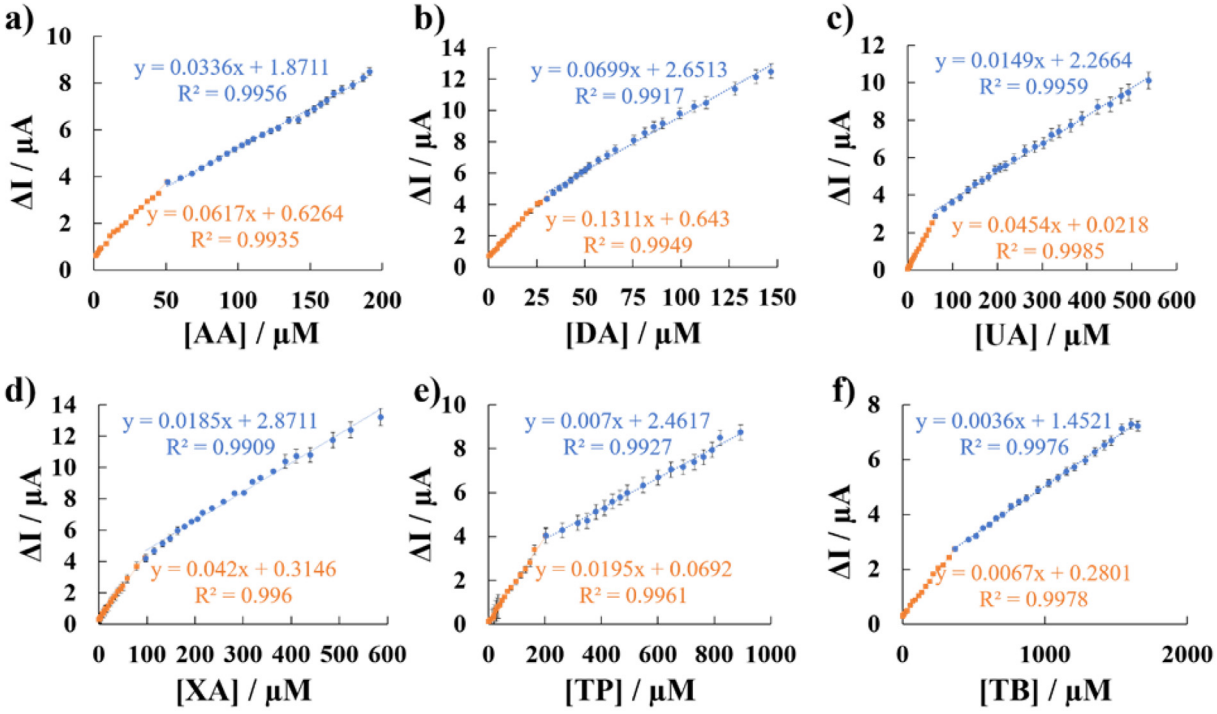

Fig. 6. The plots for the concentration dependence of increasing anodic peak current signals for (a) AA, (b) DA, (c) UA, (d) XA, (e) TP, and (f) TB with the linear range marked in blue and orange. (For interpretation of the references to colour in this figure legend, the reader is referred to the web version of this article.)

six biomolecules. Moreover, TiO_2NRs-MWCNTs/GCE is the second modified electrode that is reported to simultaneously detect up to six biomolecules, to the best of our knowledge.

3.7. Interference

AA, DA, UA, XA, TP and TB can coexist at varying concentrations in real-life samples. Hence the interference study of each biomolecule is important to determine whether the biomolecules can disrupt the simultaneous detection of other species in the same solution. In all experiments conducted, the concentration of one species was gradually increased while the others were kept at a constant concentration in the solution throughout the study. Fig. S1a-f shows the results of interference studies performed for each of the six biomolecules. As shown in Fig. S1a, the peak current of AA increased linearly with increasing concentrations, however, the oxidation peak currents of DA, UA, XA, TP and TB remained constant. Similarly, Fig. S1(b–f) shows the DPV signals corresponding to the oxidation of DA, UA, XA, TP, and TB, respectively, which increased linearly in response to the increasing concentration, while the anodic peak currents for all other biomolecules remained relatively constant. This indicated that the oxidation of AA, DA, UA, XA, TP, and TB at TiO_2NRs−MWCNTs/GCE took place independently and did not cause any interference.

3.8. Chronoamperometry

To determine the diffusion coefficient (D) of the six biomolecules, chronoamperometric measurements were conducted using TiO_2NRs-MWCNTs/GCE by applying a constant potential of 0.13, 0.33, 0.47, 0.83, 1.12, and 1.36 V for AA, DA, UA, XA, TP, and TB, respectively. As shown in Fig. S2(a-f), chronoamperograms

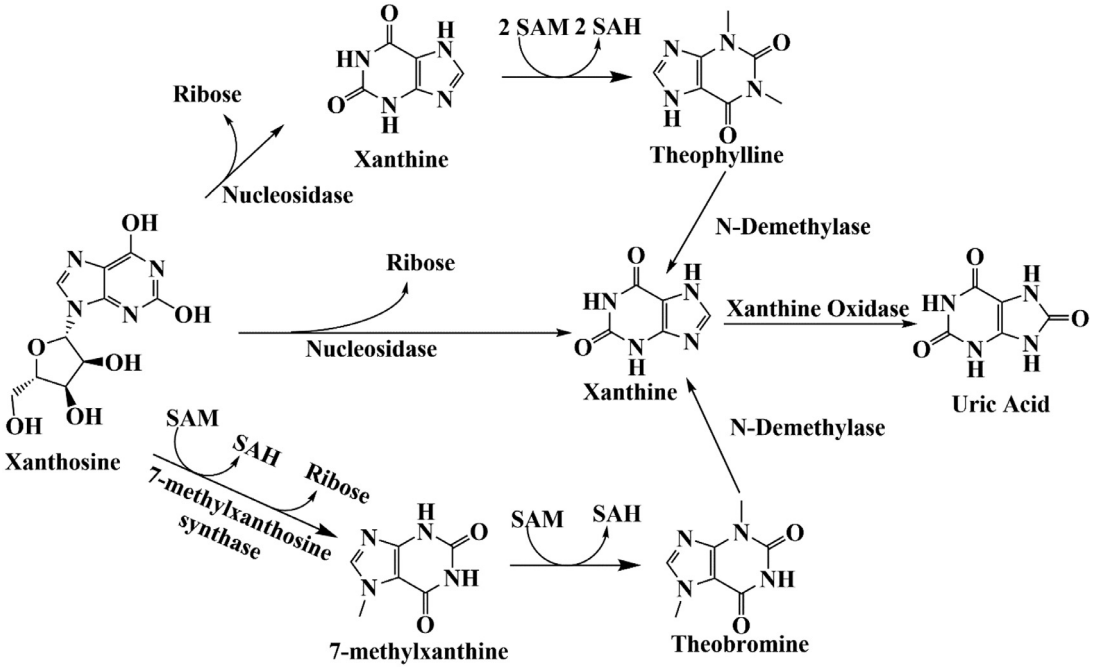

Scheme 1. Hypothesized degradation pathways for xanthosine to uric acid *via* different routes of Theophylline, Xanthine, and Theobromine.

Table 1
Analytical performance comparison between the reported modified electrochemical sensors and the TiO_2NRs-MWCNTs/GCE sensor in this work.

Analyte	Electrode	LOD (μM)	Linear range (μM)	Ref
AA	FCdCH-MWCNTs	5.26	10.0–2056.8	[25]
	AgNPs-rGO/GCE	9.6	10–800	[71]
	$[Ni(phen)_2]^{2+}$/SWCNTs/GCE	12.0	30–1546	[72]
	TiO_2NRs-MWCNTs/GCE	**0.51**	**1.5–51.0, 51.0–191.0**	**This work**
DA	FCdCH-MWCNTs	0.0011	0.99–94.1	[25]
	AgNPs-rGO/GCE	5.4	10–800	[71]
	$[Ni(phen)_2]^{2+}$/SWCNTs/GCE	1.0	1–780	[72]
	TiO_2NRs-MWCNTs/GCE	**0.06**	**0.45–30.0, 30.0–147.0**	**This work**
UA	pPABSA/GCE	0.1	1–100	[22]
	AgNPs-rGO/GCE	8.2	10–800	[71]
	$[Ni(phen)_2]^{2+}$/SWCNTs/GCE	0.8	1–1407	[72]
	TiO_2NRs-MWCNTs/GCE	**0.05**	**0.40–61.0, 61.0–537.0**	**This work**
XA	pPABSA/GCE	0.4	0.5–100	[22]
	FCdCH-MWCNTs/GPE	0.0073	1–191.27	[25]
	BDDE	–	1–100	[28]
	GCE/Nf–{RuDMSO–Cl–H2O}-MME	2.35	50–500	[73]
	TiO_2NRs-MWCNTs/GCE	**0.09**	**0.5–97.0, 97.0–586.0**	**This work**
TP	pPABSA/GCE	7.0	1- 100	[22]
	BDDE	–	1–400	[28]
	ED-GO/GCE	0.1	0.8- 60	[74]
	TiO_2NRs-MWCNTs/GCE	**0.56**	**1.0–203.0, 203.0–893.0**	**This work**
TB	BDDE	–	1–400	[28]
	BDDE	0.42	0.99–54.5	[29]
	TiO_2NRs-MWCNTs/GCE	**0.75**	**1.5–368.0, 368.0–1653.0**	**This work**

Abbreviations: FCdCH: Ferricyanide-doped chitosan;; AgNPs: Silver nanoparticles; rGO: Reduced graphene oxide; $[Ni(phen)_2]^{2+}$: Nickel(II)-bis(1,10-phenanthroline); SWCNTs: Single-walled carbon nanotubes; pPABSA: poly (para-amino benzene sulfonic acid); BDDE: Boron-doped diamond electrode; ED-GO: Electrodeposited graphene oxide.

display the current response for an electrochemical reaction which is under diffusion control as described by Cottrell's equation (Eq. (14)) [75]:

$$I = nFACD^{1/2}\pi^{-1/2}t^{-1/2} \quad (14)$$

where, n represents the number of electrons transferred, F represents Faraday's constant (96,485 C mol^{-1}), A represents the working electrode's surface area, C is the analyte concentration (mol cm^{-3}), and D is the diffusion coefficient. For a diffusion-controlled process, the plot of I *vs.* $t^{-1/2}$ would be linear and the slope ($nFAD^{1/2}C_b\pi^{-1/2}$) from the best-fit of the linear regions can be used to calculate D for AA, DA, UA, XA, TP and TB. D values were calculated to be $(6.33 \pm 0.10)\times 10^{-6}$, $(7.97 \pm 0.21)\times 10^{-6}$, $(2.65 \pm 0.17)\times 10^{-7}$, $(1.24 \pm 0.12)\times 10^{-7}$, $(5.60 \pm 0.19)\times 10^{-8}$, and $(2.97 \pm 0.15)\times 10^{-8}$ $cm^2\ s^{-1}$ for AA, DA, UA, XA, TP and TB, respectively. Furthermore, several studies in the literature have reported D values of AA, DA, UA, XA, and TP. Table S1 displays the comparison of the D values calculated in this study with the pre-

viously reported values. To the best of our knowledge, an electrochemical method has been used for the first time in this report to determine the experimental value of *D* for TB.

3.9. Repeatability and stability

The stability and repeatability of TiO_2NRs-MWCNTs/GCE was tested by performing multiple DPV measurements ($n = 10$) for simultaneous detection of AA (727 μM), DA (34 μM), UA (24 μM), XA (24 μM), TP (58 μM) and TB (97 μM). The results (Fig. S4) indicated that the standard deviations resulting from the anodic peak currents of six biomolecules were calculated to be 3.22% (AA), 2.54% (DA), 2.82% (UA), 5.19% (XA), 3.99% (TP), and 4.74% (TB). Furthermore, the stability of the TiO_2NRs-MWCNTs/GCE was examined by measuring the DPV signals for simultaneous detection of AA, DA, UA, XA, TP, and TB for a period of 1 month in 0.2 M PBS (pH 4.0). DPV measurements were performed using the same concentration of the six biomolecules. The stability of TiO_2NRs-MWCNTs/GCE was highlighted by the retained peak current (ΔI_{pa}) values for AA, DA, UA, XA, TP, and TB at 97.23, 95.38, 93.55, 98.99, 94.17, and 95.46%, respectively. These results indicated an excellent stability and repeatability of the TiO_2NRs-MWCNTs/GCE for simultaneous detection of six target biomolecules.

3.10. Scan rate

Linear sweep voltammetry (LSV) measurements were performed at varying scan rates using the TiO_2NRs-MWCNTs/GCE in a mixture of all six target biomolecules. The dependence of the peak current with different scan rates was used to determine if the electrochemical processes at the surface of the modified electrodes were diffusion- or adsorption-controlled [25,76]. Fig. S5 indicates that the anodic peak current was directly proportional to the square root of the scan rate for all six biomolecules, suggesting a diffusion-controlled process was occurring at the surface of the TiO_2NRs-MWCNTs/GCE. As shown in Fig. S5a, it was observed for each of the target biomolecule that the anodic peak current increased and the oxidation peak potential shifted to more positive values with increasing scan rates during the LSV measurements. In addition, a plot of logarithm of anodic peak current (I_{pa}) *versus* logarithm of scan rate (v) was analyzed to confirm whether the electrode process was diffusion- or adsorption-controlled (Fig. S5c). Prior literature studies have indicated that the electrocatalysis of the biomolecules at the electrode surface was significantly impacted with the slope value of log (I_{pa}) *vs.* log (v) [77]. The slope value closer to 0.5 indicated that the electrode reaction is diffusion-controlled, while the slope value closer to 1.0 indicated an adsorption-controlled process [77-80]. The relationship for log (I_p) *vs.* log (v) was found to be linear with a slope of 0.46, 0.51, 0.49, 0.52, 0.52, and 0.57 for AA, DA, UA, XA, TP and TB, respectively that was near to the theoretical value of 0.5 indicating a diffusion-controlled process [77-80].

Moreover, LSV signals indicated that AA, DA, UA, XA, TP and TB underwent an irreversible electrochemical charge transfer process [81,82]. For all the six biomolecules, since only the oxidation peak was observed, a graph showing the dependence of the anodic peak potential (E_{pa}) and the natural logarithm of the scan rate ($\ln v$) was plotted. As shown in Fig. S6, the plot followed a linear regression based on the following equation:

$$E_{pa} = (0.0424 \pm 0.002)\ln v \left(mV\ s^{-1}\right) + (0.6434 \pm 0.017)\ \left(R^2 = 0.9966\right) \quad (15)$$

For totally irreversible and diffusion-controlled electrode processes as observed for the six biomolecules, the dependence of the E_{pa} *versus* the $\ln v$ can be represented by the following a modified Laviron's equation [83]:

$$E_{pa} = E_0 + \left(\frac{RT}{\alpha nF}\right)\ln\left(\frac{RTk^0}{\alpha nF}\right) + \left(\frac{RT}{\alpha nF}\right)\ln v \quad (16)$$

where E_0 is the formal redox potential, R is gas constant, T is temperature, F is Faraday's constant, k^0 is the standard heterogeneous rate constant, α is the electron transfer coefficient, n is the number of electrons transferred, v is the scan rate. The slope from the plot of E_{pa} *versus* $\ln v$ was used to determine the value of αn. The αn for AA, DA, UA, XA, TP and TB were calculated to be 1.17, 1.08, 1.20, 1.06, 0.98, and 1.14, respectively. Generally, for an irreversible process, based on previous studies reported in literature, the α value is assumed to be 0.5 [81,82]. Therefore, the value of n was calculated to be 2.34, 2.16, 2.40, 1.96, and 2.28 for AA, DA, UA, XA, TP and TB, respectively. All the obtained values could be rounded to 2 electrons, which would be in good agreement with the literature for the estimated number of electrons hypothesized during the oxidation of the target biomolecules.

3.11. Standard heterogeneous rate constant (k_s) for the electrochemical reactions

The standard heterogenous rate constants (k_s) of the electrochemical oxidation of AA, DA, UA, XA, TP and TB at the surface of TiO_2NRs-MWCNTs/GCE was determined using CV (Fig. S7) based on the Velasco equation (Eq. (17)) [84]:

$$k_s = 1.11D^{1/2}(E_p - E_{p/2})^{-1/2}v^{1/2} \quad (17)$$

where, D is the apparent diffusion coefficient, E_p and $E_{p/2}$ are the anodic peak potential and half-wave anodic peak potential, respectively, and v is the scan rate.

The standard heterogenous rate constant values for the six biomolecules provided quantitative information about the electrode-transfer redox reactions for AA, DA, UA, XA, TP and TB at TiO_2NRs-MWCNTs/GCE. The experimental k_s values of AA, DA, UA, XA, TP and TB were determined to be $(3.24 \pm 0.13) \times 10^{-3}$, $(4.89 \pm 0.23) \times 10^{-4}$, $(9.00 \pm 0.68) \times 10^{-3}$, $(7.97 \pm 0.50) \times 10^{-3}$, $(1.48 \pm 0.11) \times 10^{-2}$, $(1.80 \pm 0.10) \times 10^{-2}$ cm. s^{-1}, respectively.

3.12. Real sample analysis

The practical applicability of sensor was tested for simultaneous detection of six target biomolecules in complex matrices such as human urine and chocolate powder. A urine sample was obtained from a healthy individual and was used for the simultaneous detection of AA, DA, UA, XA, TP and TB using DPV. The stock urine sample was diluted five times with 0.2 M PBS (pH 4.0) and a background DPV measurement was performed. An anodic peak at 0.5 V indicated the presence of UA in the urine sample. For spiking studies, the randomized concentrations of AA, DA, UA, XA, TP, and TB were added to determine the recovery rate of the six biomolecules as shown in Table 2. Similarly, a stock solution of chocolate powder was prepared and spiked with the known concentrations of six biomolecules. The background DPV measurements were performed using the five-fold diluted solution of chocolate powder in 0.2 M PBS (pH 4.0). The voltammograms did not indicate the presence of any target analytes in the sample. As described earlier, the known concentrations of AA, DA, UA, XA, TP, and TB were added to determine the recovery of the six target biomolecules as shown in Table 2. These results demonstrated the ability of the sensor to detect all six analytes in both matrices, showing potential to use this electrode in real-life samples.

4. Conclusions

In this proof-of-concept study, a novel nanocomposite of TiO_2NRs-MWCNTs was synthesized using ultrasonication and a

Table 2
The simultaneous detection of AA, DA, UA, XA, TP and TB in human urine and breakfast essentials powder samples using TiO_2NRs-MWCNTs/GCE.

Sample matrix	Analyte	Detected*	Spiked	Found*	Recovery (%)
Human urine	AA	–	86.27	83.43 ± 3.30	96.71
	DA	–	3.27	3.13 ± 0.42	95.71
	UA	134.73 ± 3.1	4.42	139.22 ± 3.40	101.35
	XA	–	4.85	4.92 ± 0.78	101.44
	TP	–	6.57	6.67 ± 0.71	101.52
	TB	–	8.75	8.64 ± 0.88	98.74
Chocolate powder	AA	–	66.68	63.98 ± 3.13	95.95
	DA	–	5.17	5.35 ± 0.43	103.45
	UA	–	3.72	3.86 ± 0.33	103.73
	XA	–	4.97	4.81 ± 0.47	96.95
	TP	–	16.62	15.96± 0.79	96.03
	TB	–	134.29	133.40 ± 4.30	99.34

* Confidence interval for 95% probability calculated as $[\bar{x} \pm \frac{t(n-1,\alpha)}{\sqrt{n}}]$; $t_{2;0.05} = 2.92$.

hydrothermal procedure. To the best of our knowledge, this nanocomposite was used for the first time to prepare an electrochemical sensor that facilitated the simultaneous detection of six analytes - AA, DA, UA, XA, TP, and TB. GCE surfaces modified with TiO_2NRs-MWCNTs exhibited an improved electrochemical performance in peak separation and current intensity in comparison with bare GCE, MWCNTs/GCE, and TiO_2NRs/GCE. The optimal pH value for the sensor was determined to be pH 4.0, which yielded good detection limits and a wide linear range for all six analytes. Moreover, the application of the TiO_2NRs-MWCNTs/GCE was tested in real-life complex matrices by successfully detecting the six target analytes in the human urine sample and chocolate powder solutions with acceptable recovery values. With further development, TiO_2NRs-MWCNTs/GCE can become a promising tool for the simultaneous detection of redox-active biomolecules in environmental on-field pre-screening studies and quality control assays in food industry.

Declaration of Competing Interest

None.

Acknowledgements

K. K. acknowledges financial support from the Canada Research Chair Tier-2 award for “Bioelectrochemistry of Proteins” (Project no. 950–231116), Ontario Ministry of Research and Innovation (Project no. 35272), Discovery Grant (Project no. 3655) from Natural Sciences and Engineering Research Council of Canada (NSERC), and Canada Foundation for Innovation (Project no. 35272).B. R. P. is thankful for the PhD award from TD Graduate Research Scholarship in Environmental Science and Ontario Graduate Scholarship (OGS).

Supplementary materials

Supplementary material associated with this article can be found, in the online version, at doi:10.1016/j.electacta.2020.137094.

References

[1] N. Jadon, R. Jain, S. Sharma, K. Singh, Recent trends in electrochemical sensors for multianalyte detection-A review crossmark, Talanta 161 (2016) 894–916.
[2] S. Shahrokhian, M. Ghalkhani, Simultaneous voltammetric detection of ascorbic acid and uric acid at a carbon-paste modified electrode incorporating thionine-nafion ion-pair as an electron mediator, Electrochim. Acta 51 (2006) 2599–2606.
[3] A. Covarrubias-Pinto, A. Acuña, F. Beltrán, L. Torres-Díaz, M. Castro, Old Things New View, Ascorbic Acid Protects the Brain in Neurodegenerative Disorders, Int. J. Mol. Sci. 16 (2015) 28194–28217.
[4] D.I. Feig, D.-.H. Kang, R.J. Johnson, Uric Acid and Cardiovascular Risk, N. Engl. J. Med 359 (2008) 1811–1821.
[5] A. Agus, J. Planchais, H. Sokol, Gut Microbiota Regulation of Tryptophan Metabolism in Health and Disease, Cell Host Microbe 23 (2018) 716–724.
[6] M. Kobayashi, Y. Hoshinaga, N. Miura, Y. Tokuda, S. Shigeoka, A. Murai, F. Horio, Ascorbic acid deficiency decreases hepatic cytochrome P-450, especially CYP2B1/2B2, and simultaneously induces heme oxygenase-1 gene expression in scurvy-prone ODS rats, Biosci. Biotechnol. Biochem. 78 (2014) 1060–1066.
[7] G.W. Arbuthnott, J. Wickens, Space, time and dopamine, Trends Neurosci 30 (2007) 62–69.
[8] M.A. Cenci, Dopamine dysregulation of movement control in L-DOPA-induced dyskinesia, Trends Neurosci 30 (2007) 236–243.
[9] H.W. Berendse, J. Booij, C.M.J.E. Francot, P.L.M. Bergmans, R. Hijman, J.C. Stoof, E.C. Wolters, Subclinical dopaminergic dysfunction in asymptomatic Parkinson’s disease patients’ relatives with a decreased sense of smell, Ann. Neurol. 50 (2001) 34–41.
[10] G.U. Höglinger, P. Rizk, M.P. Muriel, C. Duyckaerts, W.H. Oertel, I. Caille, E.C. Hirsch, Dopamine depletion impairs precursor cell proliferation in Parkinson disease, Nat. Neurosci. 7 (2004) 726–735.
[11] N.D. Volkow, G.J. Wang, S.H. Kollins, T.L. Wigal, J.H. Newcorn, F. Telang, J.S. Fowler, W. Zhu, J. Logan, Y. Ma, K. Pradhan, C. Wong, J.M. Swanson, Evaluating dopamine reward pathway in ADHD: Clinical Implications, JAMA - J. Am. Med. Assoc. 302 (2009) 1084–1091.
[12] H. Rosemeyer, The chemodiversity of purine as a constituent of natural products, Chem. Biodivers. 1 (2004) 361–401.
[13] D.H. Murgida, G.M. Bilmes, R. Erra-Balsells, A Photophysical Study of Purines and Theophylline by Using Laser-Induced Optoacoustic Spectroscopy, Photochem. Photobiol. 64 (1996) 777–784.
[14] E. Fischer, Ueber Caffeïn, Theobromin, Xanthin und Guanin, Justus Liebig’s, Ann. Der Chemie 215 (1882) 253–320.
[15] H.K. Choi, D.B. Mount, A.M. Reginato, Pathogenesis of gout, Ann. Intern. Med. 143 (2005) 499–516.
[16] S. Watanabe, Y. Kounosu, H. Shimada, A. Sakamoto, Arabidopsis xanthine dehydrogenase mutants defective in purine degradation show a compromised protective response to drought and oxidative stress, Plant Biotechnol 31 (2014) 173–178.
[17] H. Ashihara, T. Yokota, A. Crozier, Biosynthesis and catabolism of purine alkaloids, in: Adv. Bot. Res., Academic Press Inc, 2013, pp. 111–138.
[18] K.D. Georgiev, M. Radeva-Ilieva, S. Stoeva, I. Zhelev, Isolation, analysis and *in vitro* assessment of CYP3A4 inhibition by methylxanthines extracted from Pu-erh and Bancha tea leaves, Sci. Rep. (2019) 9.
[19] A. Onãtibia-Astibia, E. Martínez-Pinilla, R. Franco, The potential of methylxanthine-based therapies in pediatric respiratory tract diseases, Respir. Med. 112 (2016) 1–9.
[20] H.V.S. Ganesh, M. Noroozifar, K. Kerman, Epigallocatechin gallate-modified graphite paste electrode for simultaneous detection of redox-active biomolecules, Sensors 18 (2018) 23.
[21] Z.O. Shastan, H.V.S. Ganesh, M. Noroozifar, K. Kerman, Carbon ceramic microelectrodes modified with buckyballs for simultaneous determination of redox-active biomolecules, RSC Adv. 8 (2018) 5960–5966.
[22] S. Jesny, K. Girish Kumar, Non-enzymatic Electrochemical Sensor for the Simultaneous Determination of Xanthine, its Methyl Derivatives Theophylline and Caffeine as well as its Metabolite Uric Acid, Electroanalysis 29 (2017) 1828–1837.
[23] H. Ibrahim, Y. Temerk, Sensitive electrochemical sensor for simultaneous determination of uric acid and xanthine in human biological fluids based on the nano-boron doped ceria modified glassy carbon paste electrode, J. Electroanal. Chem. 780 (2016) 176–186.
[24] X. Wang, D. Gao, M. Li, H. Li, C. Li, X. Wu, B. Yang, CVD graphene as an electrochemical sensing platform for simultaneous detection of biomolecules, Sci. Rep. 7 (2017) 7044.
[25] S. Li, M. Noroozifar, K. Kerman, Nanocomposite of ferricyanide-doped chitosan with multi-walled carbon nanotubes for simultaneous senary detection of redox-active biomolecules, J, Electroanal. Chem. 849 (2019) 113376.

[26] A. Meyer, T. Ngiruwonsanga, G. Henze, Determination of adenine, caffeine, theophylline and theobromine by HPLC with amperometric detection, Fresenius. J. Anal. Chem. 356 (1996) 284–287.

[27] H. Sereshti, M. Khosraviani, S. Samadi, M.S. Amini-Fazl, Simultaneous determination of theophylline, theobromine and caffeine in different tea beverages by graphene-oxide based ultrasonic-assisted dispersive micro solid-phase extraction combined with HPLC-UV, RSC Adv. 4 (2014) 47114–47120.

[28] N. Spătaru, B.V. Sarada, D.A. Tryk, A. Fujishima, Anodic voltammetry of xanthine, theophylline, theobromine and caffeine at conductive diamond electrodes and its analytical application, Electroanalysis 14 (2002) 721–728.

[29] Ľ. Švorc, M. Haššo, O. Sarakhman, K. Kianičková, D.M. Stanković, P. Otřísal, A progressive electrochemical sensor for food quality control: Reliable determination of theobromine in chocolate products using a miniaturized boron–doped diamond electrode, Microchem. J. 142 (2018) 297–304.

[30] N.S. Punde, A.S. Rajpurohit, A.K. Srivastava, Sensitive electrochemical platform based on nano-cylindrical strontium titanate/N-doped graphene hybrid composite for simultaneous detection of diphenhydramine and bromhexine, Electrochim. Acta 319 (2019) 727–739.

[31] P. Chen, R.L. McCreery, Control of Electron Transfer Kinetics at Glassy Carbon Electrodes by Specific Surface Modification, Anal. Chem. 68 (1996) 3958–3965.

[32] J. Bai, B. Zhou, Titanium dioxide nanomaterials for sensor applications, Chem. Rev. 114 (2014) 10131–10176.

[33] A. Ghicov, P. Schmuki, Self-ordering electrochemistry, A review on growth and functionality of TiO_2 nanotubes and other self-aligned MOx structures, Chem. Commun. (2009) 2791–2808.

[34] Y.H. Jung, K.H. Park, J.S. Oh, D.H. Kim, C.K. Hong, Effect of TiO_2 rutile nanorods on the photoelectrodes of dye-sensitized solar cells, Nanoscale Res. Lett. 8 (2013) 37.

[35] N.B. Ashoka, B.E.K. Swamy, H. Jayadevappa, Nanorod TiO_2 sensor for dopamine: A voltammetric study, New J. Chem. 41 (2017) 11817–11827.

[36] X.C. Lu, L. Song, T.T. Ding, Y.L. Lin, C.X. Xu, CuS–MWCNT based electrochemical sensor for sensitive detection of bisphenol A, Russ. J. Electrochem 53 (2017) 366–373.

[37] Z. Zhu, L. Garcia-Gancedo, A.J. Flewitt, H. Xie, F. Moussy, W.I. Milne, A critical review of glucose biosensors based on carbon nanomaterials: Carbon nanotubes and graphene, Sensors 12 (2012) 5996–6022.

[38] K. Zarei, H. Helli, Electrochemical determination of aminopyrene on glassy carbon electrode modified with multi-walled carbon nanotube-sodium dodecyl sulfate/Nafion composite film, J. Electroanal. Chem. 749 (2015) 10–15.

[39] J. Chlistunoff, J.M. Sansiñena, On the use of Nafion® in electrochemical studies of carbon supported oxygen reduction catalysts in aqueous media, J. Electroanal. Chem. 780 (2016) 134–146.

[40] S. Tarahomi, G. Hossein Rounaghi, M. Hossein Arbab Zavar, L. Daneshvar, Electrochemical Sensor Based on TiO_2 Nanoparticles/Nafion Biocompatible Film Modified Glassy Carbon Electrode for Carbamazepine Determination in Pharmaceutical and Urine Samples, J. Electrochem. Soc. 165 (2018) 946–952.

[41] V.B. Koli, A.G. Dhodamani, A.V. Raut, N.D. Thorat, S.H. Pawar, S.D. Delekar, Visible light photo-induced antibacterial activity of TiO_2-MWCNTs nanocomposites with varying the contents of MWCNTs, J. Photochem. Photobiol. A Chem. 328 (2016) 50–58.

[42] S.D. Delekar, A.G. Dhodamani, K.V. More, T.D. Dongale, R.K. Kamat, S.F.A. Acquah, N.S. Dalal, D.K. Panda, Structural and Optical Properties of Nanocrystalline TiO_2 with Multiwalled Carbon Nanotubes and Its Photovoltaic Studies Using Ru(II) Sensitizers, ACS Omega 3 (2018) 2743–2756.

[43] K.E. Karakitsou, X.E. Verykios, Effects of altervalent cation doping of TiO_2 on its performance as a photocatalyst for water cleavage, J. Phys. Chem. 97 (1993) 1184–1189.

[44] S. Bagheri, K. Shameli, S.B. Abd Hamid, Synthesis and characterization of anatase titanium dioxide nanoparticles using egg white solution via Sol-Gel method, J. Chem 2013 (2013) 848205.

[45] L.S. Chougala, M.S. Yatnatti, R.K. Linganagoudar, R.R. Kamble, J.S. Kadadevarmath, A simple approach on synthesis of TiO_2 nanoparticles and its application in dye sensitized solar cells, J. Nano- Electron. Phys. 9 (2017) 04005.

[46] B.R. Patel, M. Noroozifar, K. Kerman, Review — Nanocomposite-Based Sensors for Voltammetric Detection of Hazardous Phenolic Pollutants in Water, J. Electrochem. Soc. 167 (2020) 037568.

[47] P. Krzyczmonik, E. Socha, S. Skrzypek, K. Soliwoda, G. Celichowski, J. Grobelny, Honeycomb-structured porous poly(3,4-ethylenedioxythiophene) composite layers on a gold electrode, Thin Solid Films 565 (2014) 54–61.

[48] F. Kaedi, Z. Yavari, M. Asmaei, A.R. Abbasian, M. Noroozifar, Ethanol electrooxidation on high-performance mesoporous $ZnFe_2O_4$-supported palladium nanoparticles, New J. Chem. 43 (2019) 3884–3890.

[49] K. Cinková, K. Kianičková, D.M. Stanković, M. Vojs, M. Marton, L. Švorc, The doping level of boron-doped diamond electrodes affects the voltammetric sensing of uric acid, Anal. Methods 10 (2018) 991–996.

[50] K. Cinková, N. Zbojeková, M. Vojs, M. Marton, A. Samphao, Švorc, Electroanalytical application of a boron-doped diamond electrode for sensitive voltammetric determination of theophylline in pharmaceutical dosages and human urine, Anal. Methods 7 (2015) 6755–6763.

[51] M. Shahbakhsh, M. Noroozifar, Copper polydopamine complex/multiwalled carbon nanotubes as novel modifier for simultaneous electrochemical determination of ascorbic acid, dopamine, acetaminophen, nitrite and xanthine, J. Solid State Electrochem 22 (2018) 3049–3057.

[52] A. Carolina Torres, M.M. Barsan, C.M.A. Brett, Simple electrochemical sensor for caffeine based on carbon and Nafion-modified carbon electrodes, Food Chem 149 (2014) 215–220.

[53] L. Švorc, Determination of caffeine: A comprehensive review on electrochemical methods, Int. J. Electrochem. Sci. 8 (2013) 5755–5773.

[54] B.R. Patel, M. Noroozifar, K. Kerman, Prussian blue-doped nanosized polyaniline for electrochemical detection of benzenediol isomers, Anal. Bioanal. Chem. 412 (2020) 1769–1784.

[55] F. Shang, Y. Liu, S. Hrapovic, J.D. Glennon, J.H.T. Luong, Selective detection of dopamine using a combined permselective film of electropolymerized (poly–tyramine and poly-pyrrole-1-propionic acid) on a boron-doped diamond electrode, Analyst 134 (2009) 519–527.

[56] E.Y. Andreeva, S.G. Dmitrienko, Y.A. Zolotov, Methylxanthines: Properties and determination in various objects, Russ. Chem. Rev. 81 (2012) 397–414.

[57] M.C. Gennaro, C. Abrigo, P. Biglino, Quantification of theophylline in human plasma by reversed-phase ion-interaction high-performance liquid chromatography and comparison with the TDx fluorescence polarization immunoassay procedure, Analyst 117 (1992) 1071–1074.

[58] R. Fu, C.J. Chen, H.A. Jinnah, Genotypic and phenotypic spectrum in attenuated variants of lesch-nyhan disease, Mol. Genet. Metab. 112 (2014) 280–285.

[59] W. Sroysee, S. Chairam, M. Amatatongchai, P. Jarujamrus, S. Tamuang, S. Pimmongkol, L. Chaicharoenwimolkul, E. Somsook, Poly(m-ferrocenylaniline) modified carbon nanotubes-paste electrode encapsulated in nafion film for selective and sensitive determination of dopamine and uric acid in the presence of ascorbic acid, J. Saudi Chem. Soc. 22 (2018) 173–182.

[60] A.A. Ensafi, M. Taei, T. Khayamian, Simultaneous determination of ascorbic acid, dopamine, and uric acid by differential pulse voltammetry using tiron modified glassy carbon electrode, Int. J. Electrochem. Sci. 5 (2010) 116–130.

[61] J. Cheng, X. Wang, T. Nie, L. Yin, S. Wang, Y. Zhao, H. Wu, H. Mei, A novel electrochemical sensing platform for detection of dopamine based on gold nanobipyramid/multi-walled carbon nanotube hybrids, Anal. Bioanal. Chem. 412 (2020) 2433–2441.

[62] M. Mazloum-Ardakani, H. Rajabi, H. Beitollahi, B.B.F. Mirjalili, A. Akbari, N. Taghavinia, Voltammetric determination of dopamine at the surface of TiO_2 nanoparticles modified carbon paste electrode, Int. J. Electrochem. Sci. 5 (2010) 147–157.

[63] M. Hosseini, M.M. Momeni, M. Faraji, An innovative approach to electro-oxidation of dopamine on titanium dioxide nanotubes electrode modified by gold particles, J. Appl. Electrochem. 40 (2010) 1421–1427.

[64] S.A. Kumar, C.F. Tang, S.M. Chen, Electroanalytical determination of acetaminophen using nano-TiO_2/polymer coated electrode in the presence of dopamine, Talanta 76 (2008) 997–1005.

[65] S. Alwarappan, G. Liu, C.Z. Li, Simultaneous detection of dopamine, ascorbic acid, and uric acid at electrochemically pretreated carbon nanotube biosensors, Nanomedicine Nanotechnology, Biol. Med. 6 (2010) 52–57.

[66] N. Mohammed Modawe Alshik Edris, J. Abdullah, S. Kamaruzaman, M.I. Saiman, Y. Sulaiman, Electrochemical reduced graphene oxide-poly(eriochrome black T)/gold nanoparticles modified glassy carbon electrode for simultaneous determination of ascorbic acid, dopamine and uric acid, Arab. J. Chem. 11 (2018) 1301–1312.

[67] X. Zhou, N. Zheng, S. Hou, X. Li, Z. Yuan, Selective determination of dopamine in the presence of ascorbic acid at a multi-wall carbon nanotube-poly(3,5-dihydroxy benzoic acid) film modified electrode, J. Electroanal. Chem. 642 (2010) 30–34.

[68] A.R. Rajamani, R. Kannan, S. Krishnan, S. Ramakrishnan, S.M. Raj, D. Kumaresan, N. Kothurkar, M. Rangarajan, Electrochemical sensing of dopamine, uric acid and ascorbic acid using tRGO-TiO_2 nanocomposites, J. Nanosci. Nanotechnol. 15 (2015) 5042–5047.

[69] B.L. Hanssen, S. Siraj, D.K.Y. Wong, Recent strategies to minimise fouling in electrochemical detection systems, Rev. Anal. Chem. 35 (2016) 1–28.

[70] G. Li, S. Yang, L. Qu, R. Yang, J. Li, Simultaneous voltammetric determination of ascorbic acid and uric acid using a Nafion/multi-wall carbon nanotubes composite film-modified electrode, J. Solid State Electrochem 15 (2011) 161–166.

[71] B. Kaur, T. Pandiyan, B. Satpati, R. Srivastava, Simultaneous and sensitive determination of ascorbic acid, dopamine, uric acid, and tryptophan with silver nanoparticles-decorated reduced graphene oxide modified electrode, Coll. Surf. B Biointerfaces 111 (2013) 97–106.

[72] S. Yan, X. Li, Y. Xiong, M. Wang, L. Yang, X. Liu, X. Li, L.A.M. Alshahrani, P. Liu, C. Zhang, Simultaneous determination of ascorbic acid, dopamine and uric acid using a glassy carbon electrode modified with the nickel(II)-bis(1,10-phenanthroline) complex and single-walled carbon nanotubes, Microchim. Acta 183 (2016) 1401–1408.

[73] A.S. Kumar, P. Swetha, $Ru(DMSO)_4Cl_2$ nano-aggregated Nafion membrane modified electrode for simultaneous electrochemical detection of hypoxanthine, xanthine and uric acid, J. Electroanal. Chem. 642 (2010) 135–142.

[74] F. Cui, X. Zhang, A method based on electrodeposition of reduced graphene oxide on glassy carbon electrode for sensitive detection of theophylline, J. Solid State Electrochem 17 (2013) 167–173.

[75] A.J. Bard, L.R. Faulkner, Kinetics of electrode reactions, Electrochem. Methods Fundam. Appl. (2001) 91–92 2nd ed., New York.

[76] N. Sabbaghi, M. Noroozifar, Nanoraspberry-like copper/ reduced graphene oxide as new modifier for simultaneous determination of benzenediols isomers and nitrite, Anal. Chim. Acta 1056 (2019) 16–25.

[77] Y. Zhou, W. Tang, J. Wang, G. Zhang, S. Chai, L. Zhang, T. Liu, Selective determination of dopamine and uric acid using electrochemical sensor based on poly(alizarin yellow R) film-modified electrode, Anal. Methods 6 (2014) 3474–3481.

[78] A.K. Timbola, C.D. Souza, C. Soldi, M.G. Pizzolatti, A. Spinelli, Electro-oxidation of rutin in the presence of p-toluenesulfinic acid, J. Appl. Electrochem. 37 (2007) 617–624.
[79] J. Wang, Analytical Electrochemistry, 2 ed., John Wiley & Sons, Inc., Hoboken, NJ, 2006.
[80] D. Thomas, Z. Rasheed, J.S. Jagan, K.G. Kumar, Study of kinetic parameters and development of a voltammetric sensor for the determination of butylated hydroxyanisole (BHA) in oil samples, J. Food Sci. Technol. 52 (2015) 6719–6726.
[81] X. Yan, C. Zhou, Y. Yan, Y. Zhu, A Simple and Renewable Nanoporous Gold-based Electrochemical Sensor for Bisphenol A Detection, Electroanalysis 27 (2015) 2718–2724.
[82] S.A. Shahamirifard, M. Ghaedi, Z. Razmi, S. Hajati, A simple ultrasensitive electrochemical sensor for simultaneous determination of gallic acid and uric acid in human urine and fruit juices based on zirconia-choline chloride-gold nanoparticles-modified carbon paste electrode, Biosens. Bioelectron. 114 (2018) 30–36.
[83] E. Laviron, General expression of the linear potential sweep voltammogram in the case of diffusionless electrochemical systems, J. Electroanal. Chem. 101 (1979) 19–28.
[84] J.G. Velasco, Determination of standard rate constants for electrochemical irreversible processes from linear sweep voltammograms, Electroanalysis 9 (1997) 880–882.